Journal of Nanoparticle Research (2006) 8: 429–443
DOI 10.1007/s11051-005-9009-x

Preparation of magnetic nanoparticles by pulsed plasma chemical vapor synthesis

I. Matsui[1,2,*]
[1]*Japan Chemical Innovation Institute, Kandajinbo-cho, chiyoda-ku, Tokyo, Japan;* [2]*Toshiba Corporate Research and Development Center, Komukaitoshiba-cho 1, Kawasaki, Japan; *Author for correspondence (Tel.: +81-3-5841-7398; E-mail: imats@chemsys.t.u-tokyo.ac.jp)*

Received 30 June 2005; accepted in revised form 6 July 2005

Key words: chemical vapor synthesis, glow discharge plasma, magnetic nanoparticle, FePt, magnetization, aerosols

Abstract

FePt nanoparticle is expected as a candidate for the magnetic material of the high density recording media. We attempted to synthesize FePt alloy nanoparticles using 13.56 MHz glow discharge plasma with the pulse operation of a square-wave on/off cycle of plasma discharge to control the size of nanoparticles. Vapors of metal organics, Biscyclopentadienyl iron (ferrocene) for Fe and (Methylcyclopentadienyl) trimethyl platinum for Pt, were introduced into the capacitively coupled flow-through plasma chamber, which consisted of shower head RF electrode and grounded mesh electrode. Synthesis experiments were conducted at room temperature under the conditions of pressure 0.27 Pa, source gas concentration 0.005 Pa, gas residence time 0.5 s and plasma powers 60 watts. Pulse width for plasma duration was chosen from 0.5 to 30 s and plasma off period was 4 s to each pulse operation. Visual observations during the particle growth showed plasma emission in the bulk region was increased with the particle growth. These were theoretically explained by using the model for both transient particle charging in the plasma and single particle behavior in the stationary plasma as well as assuming the similarity between the negative charged particle and negative gas containing plasma. Synthesized nanoparticles were directly collected onto TEM grid, which was placed just below the grounded mesh electrode in the plasma reactor downstream. TEM pictures showed two kinds of particles in size, one of which was nanometer size and isolated with crystal structures and the other appeared agglomerate of nanometer size particles. The size of agglomerated particle was controlled in the 10–120 nm range by varying the plasma-on time from 0.5 to 30 s, although the nanometer size particles did not change. The composition of FePt alloy particles could be altered by adjusting the source gas feed ratio. Also magnetization of FePt nanoparticles was measured by use of SQUID (superconducting quantum interference device) magnetometry measurements. As-synthesized FePt nanoparticles did not exhibit loop-shape characteristic, which indicated superpamagnetic property. Annealed nanoparticles with the composition of $Fe_{58}Pt_{42}$ at 650°C in atmospheric hydrogen showed clear hysterisis loop with the coercivity as large as 10 KOe.

Nomenclature

d_p	particle diameter [m]	e	unit charge [C]
D_e	diffusion coefficient for electron [m^2/s]	F	force [N]
D_I	diffusion coefficient for ion [m^2/s]	H_C	coercivity [Oe]

K_n	Knudsen number [-]
k	Boltzman constant [J/K]
m_i	ion mass [kg]
n_e	number concentration of electron [1/m^3]
n_I	number concentration of ion [1/m^3]
n_p	number concentration of particle [1/m^3]
Q_P	particle surface potential [V]
S_e	source term for elelctron [1/m^3 s]
S_I	source term for ion [1/m^3 s]
T_e	electron temperature [K]
T_I	ion temperature [K]
v_f	gas velocity [m/s]
subscript i	ion velocity [m/s]
subscript P	particle velocity [m/s]
V	electric potential [V]

Greek letters

ε_0	vacuum permittivity [F/m]
μ_e	electron mobility [m^2/Vs]
μ_I	ion mobility [m^2/Vs]
ρ_f	fluid mass density [kg/m^3]
ρ_P	particle mass density [kg/m^3]
Φ_e	electron flux [1/m^2 s]
Φ_I	ion flux [1/m^2 s]
subscript P	particle surface charge potential [V]
σ_{ID}	cross section for ion-particle momentum transfer

Introduction

Many attentions have been focused on nanoparticles, since the nanoparticles are greatly expected as novel materials for various devices, such as memory, battery, display and so on (Alivisatos, 1997; Bawendi, 1998; Kruis et al., 1998; Williams et al., 2000). Among them, nanoparticle usage for magnetic media is thought to be one of the most promising applications for nanoparticle technology. Recently IBM group presented the possibility of chemically synthesized nanoparticle for Terabit scale high-density magnetic storage media, where they showed chemically synthesized FePt nanoparticle has large coercivity compared to conventional cobalt alloys magnetic materials (Sun et al., 2000). Although liquid phase chemical synthesis is suitable for precise control for particle size, practically there have been several issues, such as the difficulty to obtain the highly pure and surfactant free particle, the scale-up problem for continuous operation and the process connectivity to existing dry process for thin film device making.

On the contrary to the liquid phase chemical synthesis technique, gas phase process, such as chemical vapor synthesis similar to Chemical Vapor Deposition (CVD), is very advantageous for contamination control of highly pure materials and for process connectivity to thin film devices, since CVD is widely recognized as one of the most important technologies in the LSI industry. There are several attempts to synthesize nanoparticles by chemical vapor synthesis (Komiyama et al., 1984; Okuyama et al., 1986; Haas et al., 1997). In most cases, chemical vapor synthesized nanoparticles are sintered and it is quite difficult to obtain the isolated nanoparticles (Seto et al., 1997). One of the key points to utilize chemical vapor synthesis for nanoparticle synthesis is to reduce the particle sintering in the reactor.

Several years ago many researches were performed on the particle behavior in the glow discharge plasma, since the plasma processes were considered as contamination source for LSI processes and named as 'dusty plasma' (Selwyn et al., 1991; Gardscadden et al., 1994; Shiratani et al., 1996). These researches elucidated the particles are negatively charged in the glow discharge region and each particles are isolated because of electrostatic force between them. Examples of particle charging and isolations were typically shown in plasma coulomb crystal (Hayashi & Tachibana, 1996; Pieper et al., 1996). The characteristic feature of dusty plasma reactors offers a convenient way to synthesize particles at submicron levels (Boufendi et al., 1996; Hayashi & Tachibana, 1996; Vivet et al., 1998; Bapat et al., 2003; Shen et al., 2003; Dong et al., 2004).

This concept can be applied to the synthesis of FePt alloy nanoparticle. Here we show an attempt to synthesize FePt nanoparticles for high-density magnetic media by plasma chemical vapor synthesis method. One of our objectives is to elucidate the possibility of plasma chemical vapor synthesis process for functional nanoparticle synthesis. Capacitively coupled plasma was operated with a

square-wave on/off cycle with various plasma durations to control the size of nanoparticles. We observed the plasma emission during the particle synthesis and measured the size and morphology of synthesized particles by TEM. The results of the visual observations were compared with theoretical model and the particle behavior was considered during particle growth in the plasma. The composition of the FePt particles was investigated by varying the source gas feed ratio and the FePt particle magnetization was measured by SQUID (superconducting quantum interference device). The effects of the alloy composition on FePt magnetization were investigated. Annealing of $Fe_{58}Pt_{42}$ nanoparticle at 650°C in hydrogen atmosphere was effective for realizing large coercivity of 10 KOe.

Experimental

We synthesized FePt nanoparticles by use of specially designed capacitively-coupled flow-through plasma chemical vapor synthesis reactor which could attain both the plug flow of the reactant gas thorough the reaction zone and the plasma confinement between the electrodes. Figure 1 shows the drawing of the reactor. The reactor consists of upper and lower electrode, quartz tube and substrate holder. Upper electrode made of stainless steel was shower-head type source gas distributor. Lower electrode was a punched stainless steel plate with 1 mm diameter hole array, pitch of which was 4 mm. The diameter of both electrodes was 32 mm and the distance between electrodes was 40 mm. RF power of 60 watts was put to the upper electrode and the lower electrode was grounded. These electrodes were equipped in the quartz glass tube, which take advantage to enable the plasma observation during the particle growth. The sample nanoparticles were collected on the silicon substrate or TEM grid, which were placed on the substrate holder just below the lower electrode.

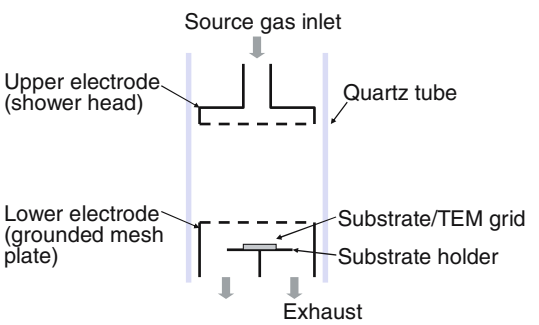

Figure 1. Enlarged view of flow-through plasma reactor.

Carrier gas was argon and the synthesis source gases were Biscyclopentadienyl iron (ferrocene) for Fe and (Methylcyclopentadienyl) trimethyl platinum for Pt. Total pressure was held at 27 Pa and source gas pressure was chosen as 0.005 Pa. The synthesis was conducted under the room temperature condition all through the synthesis. The residence time of reactant gas in the plasma region was kept at 0.5 s. The plasma was modulated with a square-wave on/off cycle of various periods. Pulse width for plasma duration was chosen from 0.5 to 30 s and plasma off period was set at 4 s to each pulse operation. Figure 2 shows the operation mode for nanoparticle synthesis. Particle size and morphology were measured by TEM and the FePt alloy composition was determined by TEM-EDX. Magnetization for the synthesized particles deposited on the silicon substrate was measured by SQUID (superconducting quantum interference device) magnetometry measurements.

Results and discussions

Visual observation of the plasma emission during particle synthesis

We observed the plasma emission between electrodes during the particle growth. Figure 3 shows the pictures of the reactor during the plasma particle synthesis. Just after the plasma input, the sheathe-bulk boundary region started to glow. Then the glowing region spread from the sheath-bulk boundary into the plasma bulk region. And finally the whole of the bulk region emitted very brightly.

Since the plasma emission is strongly scattered by the particle existence (Bouchoule & Boufendi, 1993), the above plasma glowing might be attributed to the particle growth. The above observation indicates the synthesized particles in the early stage of growth are trapped in the boundary between sheath and bulk of plasma. However, the particles

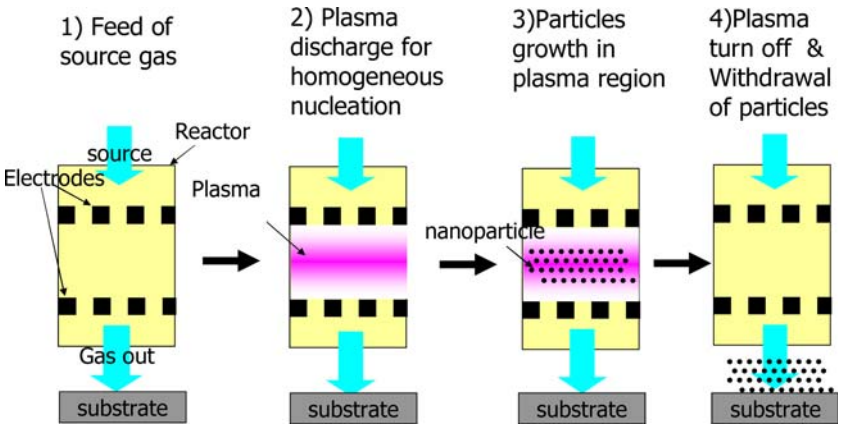

Figure 2. Operation mode of pulsed plasma chemical vapor synthesis for nanoparticle preparation.

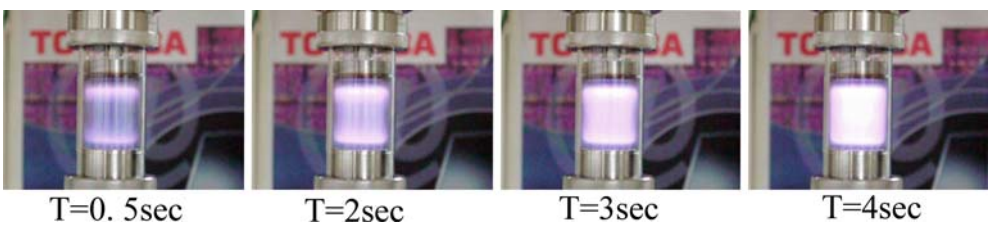

Figure 3. Plasma emission during particle growth.

do not stay the sheath-bulk boundary region for a long time and seem to move to bulk region as the particles proceed to grow. In the next part, we performed the theoretical consideration for the charging and the motion of particle in the glow discharge plasma.

Theoretical consideration on the particle behavior in the glow discharge plasma

Single particle simulation

We attempted theoretical calculation for understanding the particle behavior during particle growth on the following steps;

a. Spatiotemporal plasma structure description by gas-discharge plasma modeling.
b. Transient particle charging in glow discharge field.
c. Evaluation of the forces on the isolated charged particles in the glow discharge region.

As far as the number of the particles is limited, particle motions are less effective for gas-discharge dynamics and particle behaviors can be separately treated from the plasma spatiotemporal structure. Since the experiments were conducted under the low pressure conditions, the diffusion velocity of reactant gases is quite large compared to the gas flow. Therefore the reactant gases are thought to be completely mixed in the reactor and the following calculations are performed for spatially 1D reactor.

Capacitively coupled plasma field between electrodes was described by continuous fluid model assuming local field approximation (Boeuf, 1987). The equations describing the model are as follows, Electron conservation equation:

$$\frac{\partial n_{\mathrm{e}}}{\partial t} + \frac{\partial}{\partial x}\Phi_e = S_{\mathrm{e}} \tag{1}$$

Electron flux:

$$\Phi_e = -e\mu_e E n_{\mathrm{e}} - D_{\mathrm{e}}\frac{\partial n_{\mathrm{e}}}{\partial x} \tag{2}$$

where n_{e}, e, μ_e, E, D_{e} are electron density, unit charge, mobility for electron, electric field,

diffusion coefficient, respectively and S_e denotes source term for electron through collision reactions between electron and source gas. Ion conservation equation:

$$\frac{\partial n_{\mathrm{I}}}{\partial t}+\frac{\partial}{\partial x}\Phi_I = S_I \tag{3}$$

Ion flux:

$$\Phi_I = -e\mu_I E n_{\mathrm{I}} - D_{\mathrm{I}}\frac{\partial n_I}{\partial x} \tag{4}$$

where n_{I}, μ_I, D_{I} are ion density, mobility for ion, diffusion coefficient, respectively and S_{I} denotes source term for ion through collision reactions between electron and source gas. Electric field is correlated to the densities of electrons and ions by Poisson equation,

$$\nabla^2 V = \frac{e}{\varepsilon_0}(n_{\mathrm{e}} - n_{\mathrm{I}}) \tag{5}$$

where $E = -\frac{\partial V}{\partial x}$.

Electron and ion density distribution for Ar between electrodes were calculated and averaged during plasma cycle, where the parameters were referred to the previous study (Makabe et al., 1992). The results are given in Figure 4a and similar to the previous study (Makabe et al., 1992). Plasma is maintained by positive Ar ions (Ar^+) and electrons.

Charging of particle in the plasma could be estimated by OML (Orbital Motion Limit) model (Mott-Smith & Langmuir, 1926), considering the equation of surface potential by attached charges on the particle and the charge fluxes onto the charged particle surface (Daugherty et al., 1992; Kilgore et al., 1994).

Ion flux onto the particle:

$$I_I = \frac{e}{4}(\pi d_{\mathrm{P}}^2) n_{\mathrm{I}} c_I \frac{1}{2}\left(\exp(-u^2) + \frac{(1+2u^2+2A)}{u} erf(u)\right) \tag{6}$$

where d_{P} is particle diameter and

$$u = \frac{2}{\sqrt{\pi}}\frac{v_{i-P}}{c_I}, \quad c_{\mathrm{I}} = \left(\frac{8kT_{\mathrm{I}}}{I}\right)^{1/2}, \quad A = \frac{-e\phi_P}{kT_{\mathrm{I}}},$$

$v_{i\text{-}P}$ is the ion velocity relative to the particle velocity v_P, c_I is measure of the ion thermal speed, m_I is mass of ion, subscript P is the particle surface potential with respect to the local plasma potential, k is Botzmann constant and T_I is ion temperature and surface potential.

Electron flux onto the particle:

$$I_e = \frac{-e}{4}(\pi d_{\mathrm{P}}^2) n_{\mathrm{e}} c_e \exp\left(\frac{e\phi_P}{kT_{\mathrm{e}}}\right) \tag{7}$$

Total charge on the particle may be given by summing the ion and electron currents to the particle. Charge conservation is expressed as

$$\frac{dQ_P}{dt} = I_I + I_e \tag{8}$$

Under the conditions of interest, the charge on the particle can be expressed in terms of the surface potential through the capacitance relation (Daugherty et al., 1993) as

$$Q_P = 4\pi\varepsilon_0 d_{\mathrm{P}}\phi_P(1 + d_{\mathrm{P}}/\lambda_l) \tag{9}$$

λ_l is debye length for electron and is given as

$$\lambda_l = \left(\frac{\varepsilon_0 T_{\mathrm{e}}}{e n_{\mathrm{e}}}\right)^{1/2},$$

where ε_0 is vacuum permittivity. Assuming electron temperature is 3 eV and n_e is 10^{16} m^3, debye length was estimated as about 130 μm, which is much larger than particle diameter. Then the surface potential could be expressed as

$$Q_P = 4\pi\varepsilon_0 d_P \phi_P \tag{10}$$

By solving Eqs. (6)–(8) and (10) numerically, the transient charging of particle statically placed in the plasma could be obtained. As shown in Figure 4, we assumed plasma densities of $n_e = 10^{16}$ m^{-3} and $n_I = 10^{16}$ m^{-3} and initial condition as $Q_p = 0$ at $t = 0$. The results for particle charging with time evolution were given in Figure 5. Calculation results showed that the particle could be negatively charged with time. The time constant for charging was inversely proportional to particle size and estimated as about 100 μs for 10 nm particle, which is much larger than RF cycle time, 73 ns. This means particle charging could not follow the temporal change in the plasma discharge and it can be assumed the particle charging in the plasma would be estimated from the time averaged gas-discharge plasma. And the equilibrium number of charge on the particle was proportional to the particle diameter given in Figure 6. The number of charge 10 nm particle in the plasma was estimated as about 17

charges. Since, under our experimental conditions, the reactant gas residence time is much larger than time constant for particle charging, particles are thought to be charged in equilibrium. So the later discussions for the particle trapping are based on the time averaged plasma field and the charged particle in equilibrium.

In the above part, we obtained the information on the particle charging in the plasma. Particle motions were described by using the calculated plasma structure, considering the equation of motion of isolated particle. Equation of particle motion in the fluid is written as,

$$\frac{\pi}{6}d_{\mathrm{P}}^{3}(\rho_P+\rho_f/2)\frac{dv_P}{dt} = -C_D\frac{\overset{2}{P}\rho_f}{8C_C}(v_P-v_f)\left|v_P-v_f\right|+F_e \tag{11}$$

where d_{p} is particle diameter and ρ_P is particle density, ρ_f is fluid density, v_p is particle velocity, v_f is fluid velocity. C_D is drag coefficient to the particle from the ambient fluid. When the particle diameter is much smaller than the mean free path of the ambient gas molecule, drag coefficient can be corrected by Cunningham slip correlation factor, C_C, given as,

$$C_C = 1 + Kn(1.257 + 0.400\exp(-1.10/Kn)) \tag{12}$$

where Kn is Knudsen number.

F_e denotes the forces on the particle. We first estimated the sum of the forces onto the equilibrium charged single particle placed at each position in the stationary Ar gas plasma between electrodes. Then we compared the sum of forces from the plasma with the drag force from the flowing gas for evaluating the particle trapping behavior in the plasma.

F_e consists of gravity force, electrostatic force and ion drag force (Daugherty & Graves, 1995). These forces can be estimated separately.

Electrostatic force on the particle is given as $n_P eE$, where n_P is number density of particles, e is unit charge of electron and E is electric field.

Ion drag force is defined as the force between the positive ion and the negatively charged particles. Positive ions with a net velocity with respect to a charged particle tend to transfer momentum to the particle when the ion scatters while interacting with the electrostatic potential in the vicinity of the particle. In addition, ions that impact the particle and are collected will also transfer momentum to the particle. Ion drag force is given as $n_I\sigma_{\mathrm{ID}}m_I v_{I\text{-}P}|v_{I\text{-}P}|$, where n_I is positive ion density, σ_{ID} cross section for ion-particle momentum transfer, m_I is mass of ion and $v_{I\text{-}P}$ is net relative velocity between the positive ion and the particle (Kilgore et al., 1994). When the particle is statically placed in the plasma, $v_{I\text{-}P}$ is equivalent to ion velocity v_I, which is expressed as sum of drift and diffusion terms as,

$$v_I = \mu_I E - D_I\frac{1}{n_I}\left(\frac{\delta n_I}{\delta x}\right) \tag{13}$$

where μ_I is mobility for positive ion and D_I is diffusivity for positive ion. For Ar ion under the above plasma condition, ion plasma frequency, given as $1/2\pi\left(e^2 n_I/\varepsilon_0 m_I\right)^{1/2}$, was estimated as about 3.3 MHz, which is much smaller than RF plasma frequency of 13.56 MHz (Lieberman & Lichtenberg, 1994). Therefore ions cannot follow the periodic change in the plasma cycle and the diffusion term is dominant for the ion motion rather than the drift term.

Figure 4b shows calculated results of the sum of the forces on the 10 nm particle. In the vicinities of electrodes, the particle is pulled towards the plasma bulk by electrostatic force as about 10^{-12} N. The particle in the bulk is pulled back to the electrodes by ion drag force. It indicates there are stable points for the particle where the sum of the forces on the particle is zero between electrodes. These points nearly correspond to the boundary between sheath and bulk of plasma. Larger forces worked on larger particle of 100 nm size as shown in Figure 4c. It is expected that nanoparticle can be efficiently trapped in the plasma field during the particle growth.

Drag force from the flowing gas in Eq. (11) was estimated as about 10^{-18} N under the present experimental gas flowing condition, which was much smaller than the above estimated sum of the forces on the particle. Therefore the charged particle could be trapped and hardly flow out from the plasma reactor, which means that plasma field can be useful for the nanoparticle synthesis.

The above calculations showed that isolated particle was readily charged in the glow discharge plasma and trapped in the boundary region between sheath and bulk plasma. These calculation

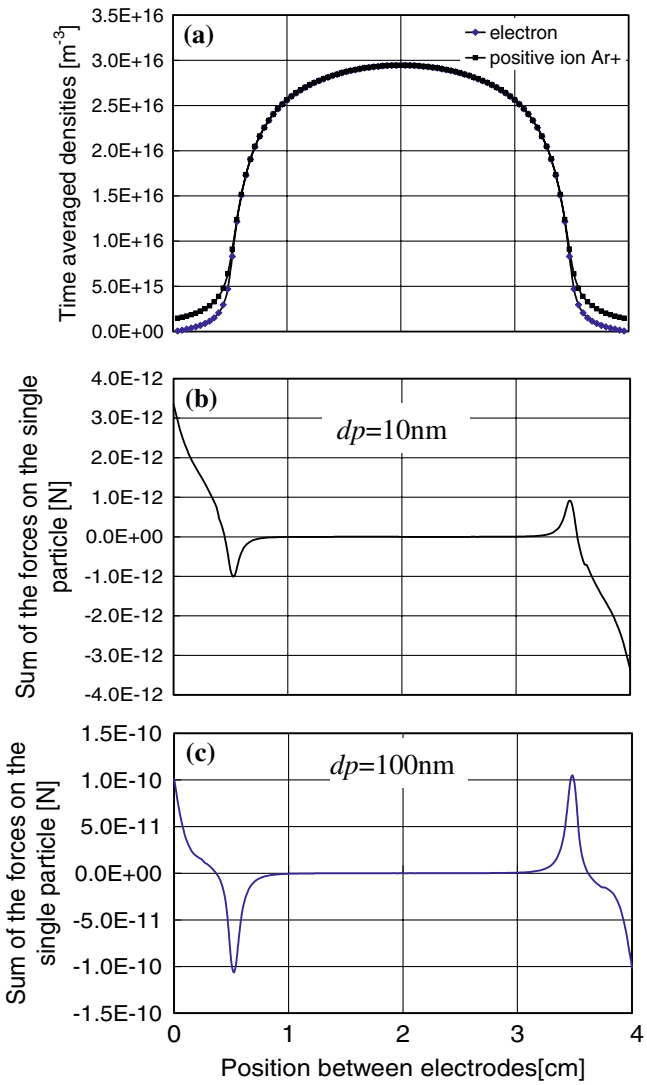

Figure 4. Calculation results describing single particle trapping in plasma: (a) electron and ion distribution in Ar plasma, (b) sum of the forces on the single particle (10 nm) placed in stationay Ar gas plasma, (c) sum of the forces on the single particle (100 nm) placed in stationay Ar gas plasma.

results correspond to the observation for the early stage of plasma particle synthesis.

Particle behavior deduced from the negative gas model

The theoretical calculation showed the number of charge on the particles was dependent on the particle size and proportional to the diameter of particles. Particles are thought to become more charged with increasing size. As a result, the amount of charge on the particles is expected to become large enough to affect the plasma field structure. Equations (1)–(5) are generally used for plasma description. Unfortunately there is not enough precise information, such as collision cross section with electron, mobility and diffusivity, on solid particles for solving the above equations. Therefore to expect the behavior of the significantly charged particles in the plasma field, here the theoretical calculation was conducted for negative gas containing plasma in place of negative charged particles, since much information have

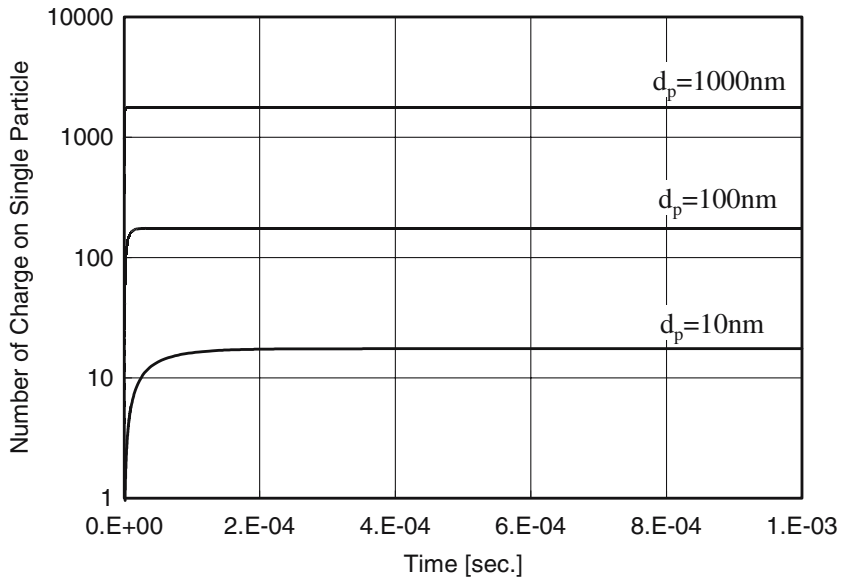

Figure 5. Transient changing of paricle in the uniform density plasma ($n_e = 10^{16}$ m^{-3}, $n_p = 10^{16}$ m^{-3}).

been obtained for discharge phenomena on the gas species rather than solid particles. O_2 was chosen as negative discharge gas, because considerable amount of the rate data for discharging are elaborately collected (Lieberman & Lichtenberg, 1994). The same calculation scheme as Ar gas plasma was used for Ar and O_2 mixture gas. Figure 7 shows the density distributions for electron, positive ion and negative ion for 1 volume% oxygen contained Ar, where the plasma conditions, such as pressure, plasma power, and distance between electrodes are same given in Figure 4. Plasma bulk region was maintained by positive ions, electrons and negative ions. Comparison of Figure 7 with Figure 4 shows the plasma field structures differ much because of negative ions in the plasma. Electron density in Figure 8 was low compared with pure Ar gas plasma and the negative ion accumulation was observed in the plasma bulk region. The density of

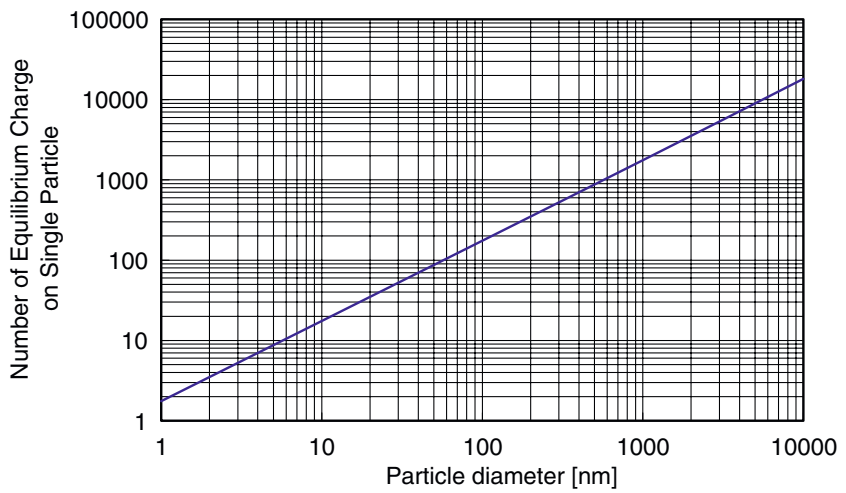

Figure 6. Equilibrium charging on single particle placed in Ar plasma ($n_e = 10^{16}$ m^{-3}, $n_p = 10^{16}$ m^{-3}).

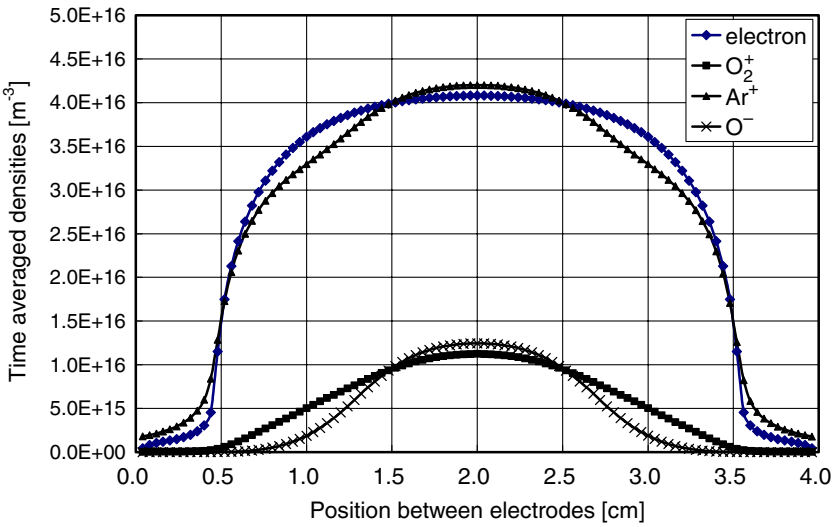

Figure 7. Time average density distributions for electrons, positive ions (O_2^+, Ar^+) and negative ions (O^-) for 1 volume% oxygen contained Ar plasma.

negative ions was estimated to be on the order of 10^{10} cm^{-3}. Particle observation by *in situ* laser-light-scattering (LLS) method performed for simultaneous measurements of size and density distributions obtained 10^8 cm^{-3} particles in the plasma region (Shiratani et al., 1996). The density of particles in our plasma reactor is much higher than 10^8 cm^{-3}, since visual observation could capture the behavior of the particles. Furthermore, during the growth, particles attach more electrons onto the surface. As a result, the sum of the charges on the particles during plasma synthesis might be on the same order of magnitude as above calculated negative ion densities. The particle accumulation into the bulk region could be explained by the negative ion behavior given in Figure 7.

Evaluations of the synthesized FePt nanoparticles

Figure 8 shows typical results of the TEM image for synsthesized FePt nanoparticles, where the plasma on-time duration of 5 s was chosen. Shape of each particle was almost spherical. The average size was about 33 nm and size distribution was less than 12%.

Figure 9a and b show the TEM pictures of nanoparticles of the plasma time duration of 2 s. Average size of particles was about 18 nm and size distribution was less than 8%. Figure 9b shows high resolution TEM picture and a close-up image of Figure 10a. We found the very small and isolated particles with about 1–2 nm size were caught entirely on TEM grid. Unfortunately size distribution for such small particles was hard to measure because of TEM resolution comstraint. But it seemed rather uniform and separated each other. These nanometer size particles showed crystal structure shown in high resolution TEM picture given in Figure 10. These syntheses were conducted under the room temperature condition. Charged species may affect on the crystallinity of the particles. Since large particles seemed to consist of smaller particles, it indicated the large particle was agglomerate of small particles.

Previous studies showed the model of particle growth in the RF plasma (Dutta et al., 1997; Fukuzawa et al., 1999). One of them is given as follows.

1. Source decomposition to produce radical species and ion species.
2. Homogeneous Nucleation and nanoparticle growth from radical and ion species.
3. Agglomeration of nanometer size particles.

This model is quite understandable but care must be paid for the particle charging in the plasma. The above theoretical calculation showed the particles

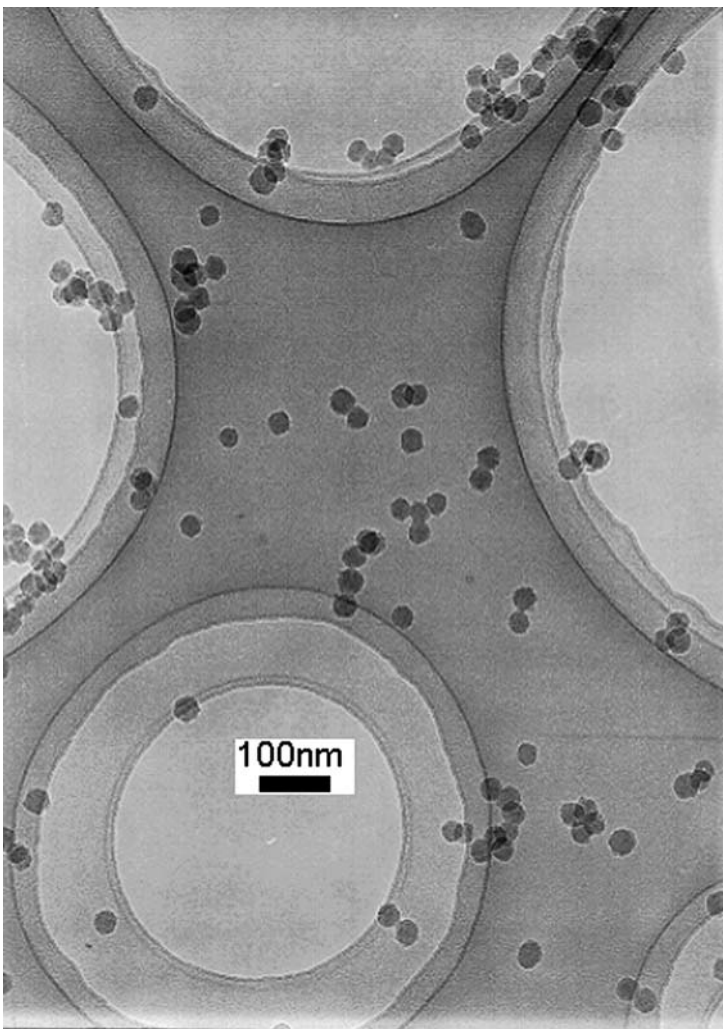

Figure 8. TEM picture of synthesised FePt nanoparticles.

in plasma are negatively charged because of large extent of electron energy in the glow discharge plasma. It is expected that the negatively charged particles are electrostatically repulsive and particle agglomerations may not occur. In Figure 9b, the small particles with a few nanometer diameter are isolated and repulsive forces are expected to work between these particles. On the contrary to these expectations, TEM pictures of large particle seem to show agglomerate of the small particles as given in Figure 9b. Since the agglomeration for nanoparticles may not occur as far as the each nanoparticle is negatively charged and electrostatically repulsive, negative charging for small particles is thought to be broken through some reasons. In the above theoretical part, we showed the results of the instantaneous negative particle charging in the time averaged uniform plasma. Here we consider either spatial non-uniformity of plasma neutrality or temporal particle charge fluctuation for particle agglomerations. Spatial non-uniformity of plasma neutrality arises in the sheath region, where there is relatively low density electron as shown in Figure 4. The charge on the particles in the vicinity of electrodes might detach from the particle surface and the particle become less negative or sometime neutral, where the particles can agglomerate each other as mentioned by Kawasaki et al. (1998). The

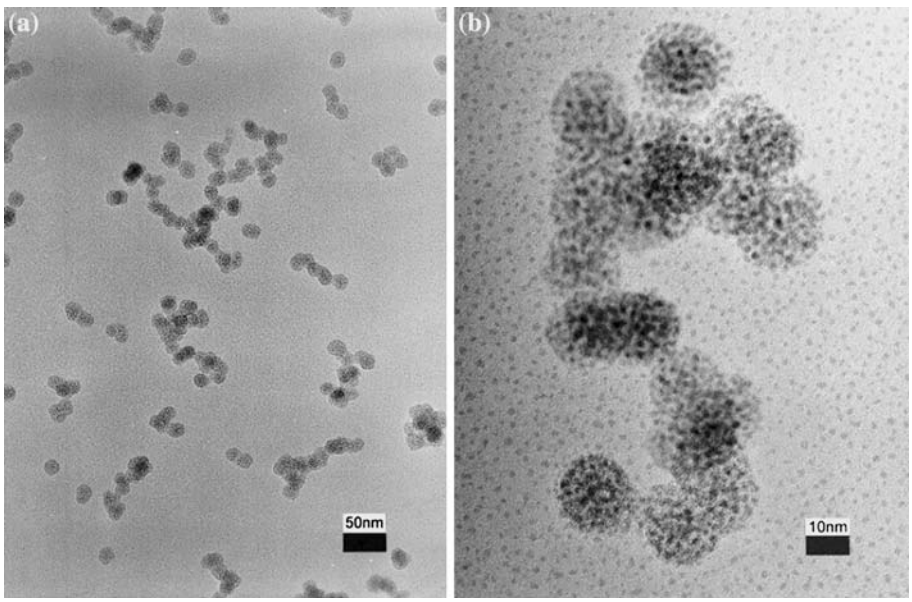

Figure 9. TEM pictures of synthesised nanoparticles (plasma duration 5 s): (a) low magnification, (b) higher magnification.

other model for negative charge breaking is based on the temporal fluctuation of charge on the particle. Previous report theoretically showed the charge on the small particle of a few nanometer is fluctuated and positive charging may take place in some time (Cui & Goree, 1994). Once the particle is positively charged, the particle instantaneously agglomerates to negative particles. Either of these models or both can explain the agglomeration of particles but the details should be studied in the future research.

We examined the effect of the plasma time duration on the particle size. As expected, when the plasma duration was small, the particle size was reduced. This tendency was consistent with the previously reported data (Bouchoule & Boufendi, 1993). We conducted the experiments to synthesize small particles as much as possible by reducing the time duration and the particle of 10 nm was obtained with plasma duration of 0.5 s. Correlation between the duration for plasma-on and the average particle size obtained is given in Figure 11. Size distribution was depending on the particle size and estimated about 8–30% to 120 to 10 nm particle, respectively.

Figure 12 shows FePt composition of nanoparticle measured by TEM-EDX in relation to source gas feed ratio. Pt content in synthesized 20 nm nanoparticles increased as the Pt source vapor pressure was increased. Although Pt was captured in the nanoparticle less effectively than Fe, FePt alloy composition could be readily controlled by adjusting the source gas feed ratio. The decomposition rates for Fe and Pt sources might differ against the electron impact in the glow discharge plasma. Although source gas for Pt, (Methylcyclopentadienyl) trimethyl platinum, contains larger size of alkaline molecule than source gas for Fe, Biscyclopentadienyl iron, electron impact cross section for decomposition might not be related to the alkaline size of molecule. Sun et al. (2001) reported the FePt nanoparticle synthesis through the thermal decomposition route in the liquid phase. Acetylacetonato platinum for Pt and iron pentacarbonyl for Fe were used as starting materials. They measured the relation between the particle composition and the molar ratio of Fe source and Pt source. The results showed not all Fe source contributed to the FePt formation. The reason was Fe source be more easily vaporized than Pt source. The choice of source materials is one of the key factors for composition control for FePt nanoparticle synthesis.

It is well known that FePt with L10 ordered phase reveals large coercivity (Tanaka et al., 1997). Magnetization for FePt nanoparticles at room

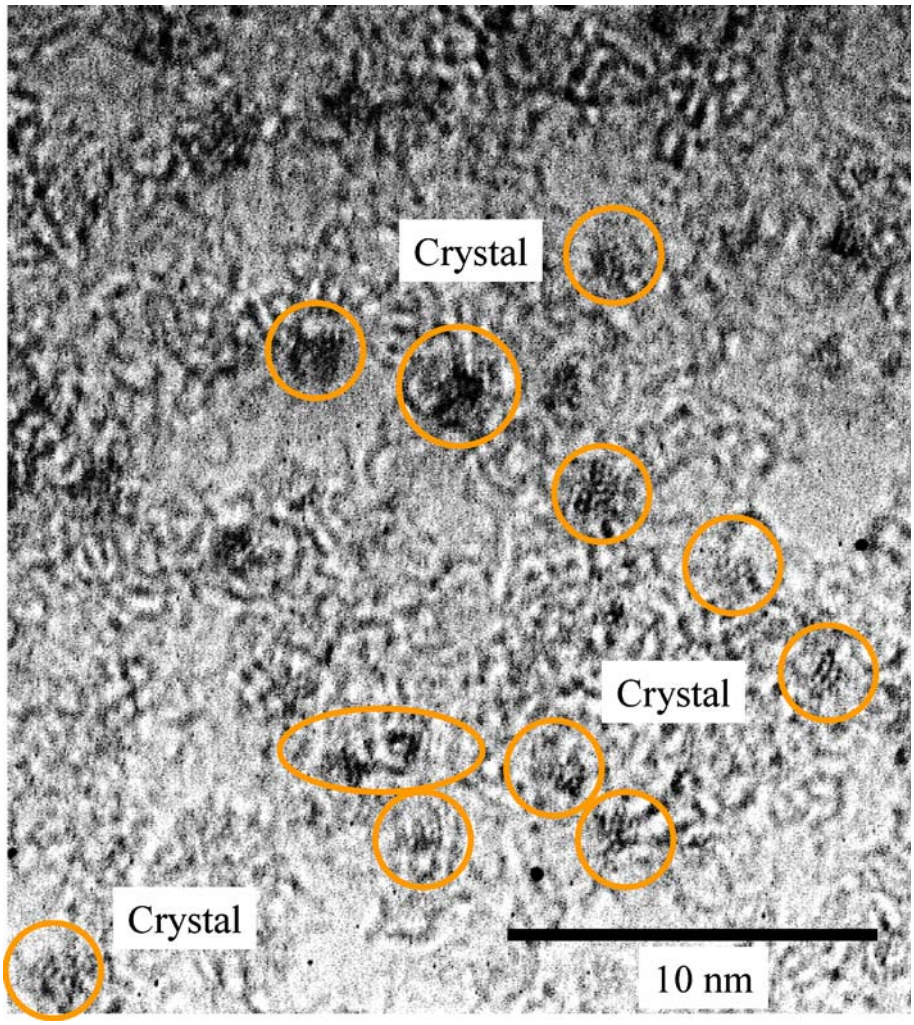

Figure 10. HRTEM images of synthesised nanoparticles.

temperature was evaluated by use of SQUID magnetometry measurements. Nanoparticle sample with the size about 20 nm were tested for magnetization. As-synthesized nanoparticle did not show loop shape characteristics, which indicated nanoparticles are superparamagnetic. Then nanoparticle samples were annealed in the closed glass tube furnace under the various atmospheres. Figure 13 shows the magnetization of the nanoparticle sample $Fe_{58}Pt_{42}$, which was annealed at 650°C for 30 min in the atmospheric hydrogen. The sample exhibited hysteresis loop and quite high coercivity as large as about 10 KOe, which is much larger than conventional cobalt alloys. These were attributed to the transformation from the fcc phase to the $L1_0$ fct phase (Sun et al., 2000). As mentioned above, as-synthesized particles have crystal structure because of charged species existing in the particle growth. This effect may not be large enough for crystal transformation from fcc to fct structure. Annealing at 800°C resulted in about 20 KOe coercivity. Annealing in nitrogen atmosphere gave no hysteretic behavior. As previously reported by Zeng et al. (2003), anneal atmosphere was important for the magnetization of FePt nanoparticles. Since the nanoparticle is very reactive to oxygen, nanoparticle exposed in the air would be readily oxidized. And also the carbonaceous materials are

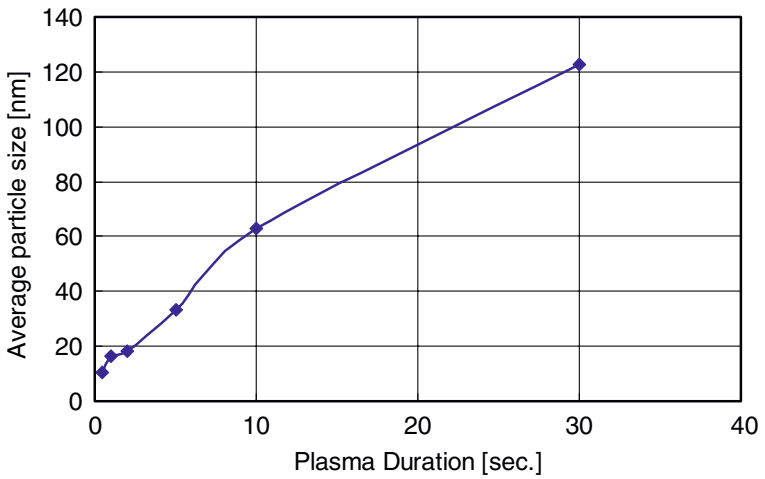

Figure 11. Relation between plasma duration and particle size.

thought to be remaining because the source gases of organometalic compounds contain certain amounts of hydrocarbons. Hydrogen played a role of reducing agent for oxidized particles as well as carbonaceous materials.

We also measured coercivity for various composition samples annealed at 650°C. Figure 14 shows the effect of the composition on the coercivity. The coercivities of these samples depended strongly on FePt composition. At about molar ratio of Fe of 58%, the very large coercivity could be obtained. As given in the phase diagram for bulk material (Massalski et al., 1996), FePt alloy has various composition phases and FePt shows magnetization from about $Fe_{35}Pt_{65}$ to $Fe_{55}Pt_{45}$. Plasma synthesized FePt nanoparticles expressed the magnetization behavior in a similar manner to the bulk metal. But there is a slight difference of FePt composition, where maximum coercivity was obtained for $Fe_{58}Pt_{42}$ sample synthesized under the present experimental conditions. This tendency is same in the chemically synthesized FePt nanoparitcles, which exhibited the maximum coercivity for the $Fe_{55}Pt_{44}$ nanoparticles (Sun

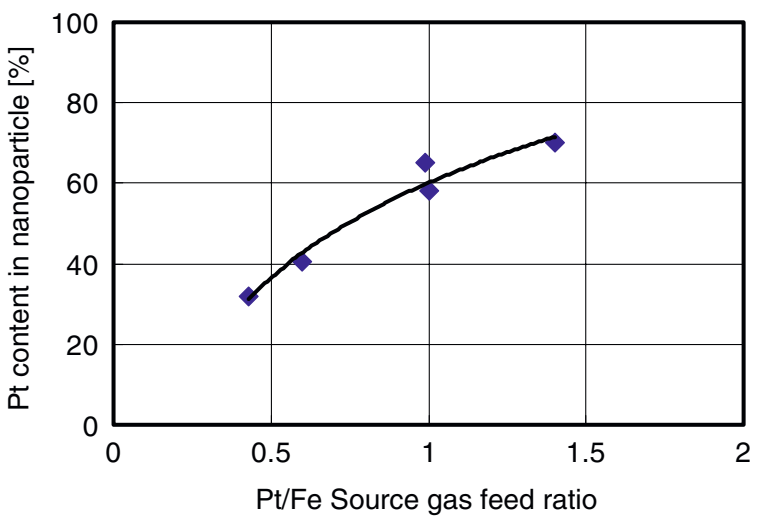

Figure 12. Relation between source gas feed ratio and Pt content in FePt nanoparticles.

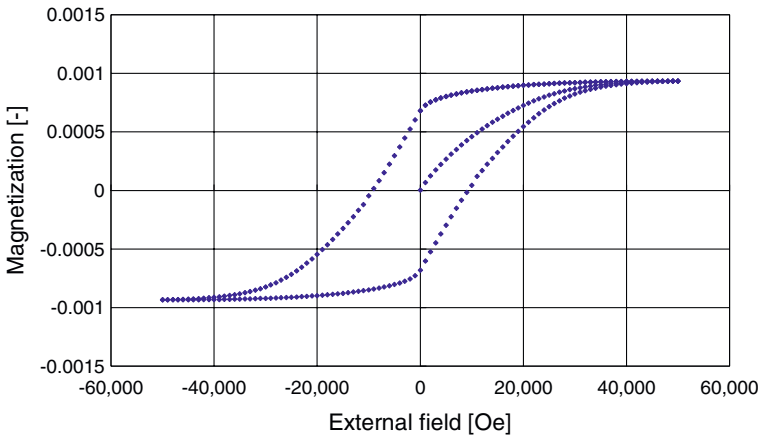

Figure 13. Typical hysterisis loop for FePt nanoparticles prepared by plasma chemical vapor synthesis.

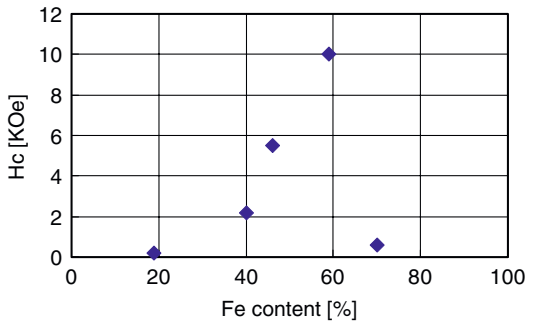

Figure 14. Relation between Fe content in FePt nanoparticles and coercivity.

et al., 2001). Although some surface effects of the nanoparticles may affect the magnetization behavior, the composition of FePt alloy was one of the most critical issues to realize large coercivity.

Conclusion

FePt nanoparticles for high-density magnetic media were synthesized by plasma chemical vapor synthesis method, where we used the capacitively coupled flow-through plasma reactor with a square-wave on/off cycle with various periods. While the particle growth proceeded, plasma emission in the region of plasma bulk was increased. These visual observations were explained by instantaneous particle charging, charged particle trapping in sheath bulk boundary and by assuming the analogous behavior between negative charged particle and negative gas plasma. Synthesized particle consisted of two kinds of particles, one was a few nanometer size particle and the other seemed to be agglomerate of nanometer-size particles. Nanometer-size particles were isolated and particle negative charging was indicated. Agglomerated particle size could be varied from 10 to 120 nm by changing the plasma-on time from 0.5 to 30 s. The composition of the FePt alloy particles was varied by changing the source gas flow ratio. The effects of the alloy composition on FePt magnetization were investigated. $Fe_{58}Pt_{42}$ nanoparticle annealed at 650°C in hydrogen atmosphere showed coercivity as large as 10 KOe. Plasma chemical vapor synthesis is thought to be one of the most interesting processes for functional nanoparticle preparation.

Acknowledgements

Financial supports from New Energy and Industrial Technology Development Organization are greatly appreciated.

References

Alivisatos A.P., 1997. Nanocrystals: Building blocks for modern materials design. Endeavour 21, 56–60.

Bapat A., C.R. Perrey, S.A. Campbell, C.B. Carter & U. Kortshagen, 2003. Synthesis of highly oriented, single-crystal

silicon nanoparticles in a low-pressure, inductively coupled plasma. J. Appl. Phys. 94, 1969–1974.
Bawendi M.G., 1998. Nanocrystalites: Building blocks for quantum dot heterostructures. Solid State Communications 107, 709.
Boeuf J.P., 1987. Numerical model of rf glow discharges. Phys. Rev. A 36, 2782–2792.
Bouchoule A. & L. Boufendi, 1993. Particulate formation and dusty plasma behavior in argon-silane RF discharge. Plasma Sources Sci. Technol. 2, 204–213.
Boufendi L., A. Bouchoule & T. Hbid, 1996. Electrical characterization and modeling of a dust forming plasma in a radio frequency discharge. J. Vac. Sci. Technol. A 14, 572–576.
Cui C. & J. Goree, 1994. Fluctuations of the charge on a dust grain in a plasma. IEEE Trans. Plasma Sci. 22, 151–158.
Daugherty J.E. & D.B. Graves, 1995. Derivation and experimental verification of a particulate transport model for a glow discharge. J. Appl. Phys. 78, 2279–2287.
Daugherty J.E., R.K. Porteous, M.D. Kilgore & D.B. Graves, 1992. Sheath structure around particles in low-pressure discharges. J. Appl. Phys. 72, 3934–3942.
Daugherty J.E., R.K. Porteous & D.B. Graves, 1993. Electrostatic forces on small particles in low-pressure discharges. J. Appl. Phys. 73, 1617–1620.
Dong Y., A. Bapat, S. Hilchie, U. Kortshagen & S.A. Campbell, 2004. The generation of free-standing single crystal silicon nanoparticles. J. Vac. Sci. Technol., B 22, 1923–1930.
Dutta J., H. Hofmann, R. Houriet, H. Hofmeister & C. Hollenstein, 1997. Growth, microstructure and sintering behavior of nanosized silicon powders. Colloids Surfaces, A 127, 263–272.
Fukuzawa T., S. Kushima, Y. Matsuoka, M. Shiratani & Y. Watanabe, 1999. Growth of particles in cluster-size range in low pressure and low power SiH_4 rf discharges. J. Appl. Phys. 86, 3543–3549.
Garscadden A., B.N. Ganguly, P.D. Haaland & J. Williams, 1994. Overview of growth and behaviour of clusters and particles in plasmas. Plasma Sources Sci. Technol. 3, 239–245.
Haas V., R. Birringer, H. Gleiter & S.E. Pratsinis, 1997. Synthesis of nanostructured powders in an aerosol flow condenser. J. Aerosol Sci. 28, 1443–1453.
Hayashi Y. & K. Tachibana, 1996. Coulomb crystal formation from growing particles in a plasma and the analysis. J. Vac. Sci. Technol. A 14, 506–510.
Kawasaki H., K. Sakamoto, S. Maeda, T. Fukuzawa, M. Shiratani & Y. Watanabe, 1998. Transition of particle growth region in SiH_4 RF discharges. Jpn. J. Appl. Phys. 37, 5757–5762.
Kilgore M.D., J.E. Daugherty, R.K. Porteous & D.B. Graves, 1994. Transport and heating of small particles in high density plasma sources. J. Vac. Sci. Technol. B 12, 486–493.
Komiyama H., T. Kanai & H. Inoue, 1984. Preparation of porous, amorphous, and ultrafine TiO2 particles by chemical vapor deposition. Chem. Let. 13, 1283–1286.
Kruis F.E., H. Fissan & A. Peled, 1998. Synthesis of nanoparticles in the gas phase for electronic, optical and magnetic applications – a review. J. Aerosol Sci. 29, 511–535.
Lieberman M.A. and A.J. Lichtenberg, Principles of plasma discharges and materials processing, 1st Ed., 1994. John Wiley & Sons.
Makabe T., N. Nakano & Y. Yamaguchi, 1992. Modeling and diagnostics of the structure of rf glow discharges in Ar at 13.56. MHz. Phys. Rev. A 45, 2520–2531.
Massalski T.B., H. Okamoto, P.R. Subramanian and L. Kacprzak, Binary Alloy Phase Diagrams, 2nd Ed., 1996. ASM international.
Mott-Smith H.M. & I. Langmuir, 1926. The theory of collectors in gaseous discharges. Phys. Rev. 28, 727–763.
Okuyama K., Y. Kousaka, N. Tohge, S. Yamamoto, J.J. Wu, R.C. Flagan & J.H. Seinfeld, 1986. Production of ultrafine metal oxide aerosol particles by thermal decomposition of metal alkoxide vapors. AIChE. J. 32, 2010–2019.
Pieper J.B., J. Goree & R.A. Quinn, 1996. Experimental studies of two-dimensional and three-dimensional structure in a crystallized dusty plasma. J. Vac. Sci. Technol. A 14, 519–524.
Selwyn G.S., J.E. Heidenreich & K.L. Haller, 1991. Rastered laser light scattering studies during plasma processing: Particle contamination trapping phenomena. J. Vac. Sci. Technol. A 9, 2817–2824.
Seto T., A. Hirota, T. Fujimoto, M. Shimada & K. Okuyama, 1997. Sintering of polydisperse nanometer-sized agglomerates. Aerosol Sci. Technol. 27, 422–438.
Shen Z., T. Kim, U. Kortshagen, P.H. McMurry & S.A. Campbell, 2003. Formation of highly uniform silicon nanoparticles in high density silane plasmas. J. Appl. Phys. 94, 2277–2283.
Shiratani M., H. Kawasaki, T. Fukuzawa & Y. Watanabe, 1996. In situ polarization-sensitive laser-light-scattering method for simultaneous measurements of two-dimensional spatial size and density distributions of particles in plasmas. J. Vac. Sci. Technol. A 14(2), 603–607.
Sun S., C.B. Murray, D. Weller, L. Folks & A. Moser, 2000. Monodisperse FePt nanoparticles and ferromagnetic FePt nanocrystal superlattices. Science 287, 1989–1992.
Sun S., E.E. Fullerton, D. Weller & C.B. Murray, 2001. Compositionally Controlled FePt Nanoparticle Materials, IEEE Trans. Magnetics 37, 1239–1243.
Tanaka Y., N. Kimura, K. Hono, K. Yasuda & T. Sakurai, 1997. Microstructures and magnetic properties of Fe–Pt permanent magnets. J. Mag. Mag. Mater. 170, 289–297.
Vivet F., A. Bouchoule & L. Boufendi, 1998. Synthesis and characterization of SiC:H ultrafine powder generated in an argon–silane–methane low-pressure radio-frequency discharge. J. Appl. Phys. 83, 7474–7481.
Williams R.S., A.P. Alivisatos, M.C. Roco, 2000. Nanotechnology Research Directions: IWGN Workshop Report. Boston, Mass.: Kluwer Academic Publ.
Zeng H., S. Sun, R.L. Sandstrom & C.B. Murray, 2003. Chemical ordering of FePt nanoparticle self-assemblies by rapid thermal annealing. J. Mag. Mag. Mater. 266, 227–232.